

Mapping large-scale anisotropy in the WMAP data

A. Bernui,^{1,*} B. Mota,^{2,†} M.J. Rebouças,^{2,‡} and R. Tavakol^{3,§}

¹*Instituto Nacional de Pesquisas Espaciais – Divisão de Astrofísica
Av. dos Astronautas 1758*

12227-010 São José dos Campos – SP, Brazil

²*Centro Brasileiro de Pesquisas Físicas
Rua Dr. Xavier Sigaud 150*

22290-180 Rio de Janeiro – RJ, Brazil

³*Astronomy Unit – School of Mathematical Sciences
Queen Mary, University of London
Mile End Road, London E1 4NS, UK*

(Dated: December 2, 2024)

Analyses of recent cosmic microwave background (CMB) observations have provided increasing indications for the existence of large scale anisotropy in the universe. Given the far reaching consequences of such an anisotropy for our understanding of the universe, it is important to employ alternative indicators in order to determine whether the reported anisotropy is cosmological in origin, and if so extract further information that may be helpful for identifying its causes. Here we propose a new directional indicator based on separation histograms of pairs of pixels with similar temperatures in the CMB map, as a measure of large scale anisotropy. The main advantage of this indicator is that it can be used to generate a sky map of large-scale anisotropies in the CMB temperature map, thus allowing a possible additional window into their causes. Using this indicator, we find a statistically significant (at 95% CL) preferred direction in the CMB data and discuss how it compares with other such axes recently reported. We also show that our findings are robust with respect to both the details of the method used, and the choice of the WMAP CMB maps employed.

PACS numbers: 98.80.Es, 98.80.-k, 98.80.Jk

I. INTRODUCTION

Recent years have witnessed a tremendous accumulation of high-precision cosmological data. In particular, the first year high precision data from the Wilkinson Microwave Anisotropy Probe (WMAP) [1] has produced a wealth of information regarding the early Universe. These have provided evidence for a nearly spatially-flat Universe with a primordial spectrum of almost scale-invariant density perturbations, as predicted by generic inflationary models. At large scales, however, a number of potentially important anomalous features in the cosmic microwave background (CMB) have been reported (see Ref. [2] for a detailed discussion), including their low quadrupole and octopole moments [3], the quadrupole-octopole axis alignment [4, 5], evidence for a North-South asymmetry [6], indications for a preferred axis of symmetry around ($b = 30^\circ, l = 250^\circ$) in galactic coordinates (with equator defined by $b = 90^\circ$), or directions of maximum asymmetry towards ($b = 100^\circ, l = 237^\circ$) [6, 7, 8, 9, 10, 11, 12, 13, 14], and also indications of non-Gaussian features in the CMB temperature fluctuations [12, 15]. Clearly the study of such anomalies must take into account the possibility that they may

have non-cosmological origins such as unsubtracted foreground contamination and/or systematics [11], unconsidered local effects like gravitational lensing [16] (see, however, Ref. [17]) or other mechanisms to break statistical isotropy [18]. They may also have extra-galactic origin [4, 6, 7, 8, 9, 10]. If they turn out to have a cosmological origin, however, they could have far reaching consequences for our understanding of the Universe, and in particular for the standard inflationary picture, which predicts statistically isotropic CMB temperature fluctuation patterns and Gaussianity.

In view of this a great deal of effort has recently gone into verifying the existence or otherwise of such anomalies, employing several different statistical approaches. Apart from corroborating the existence of a large-scale anisotropy, the utilization of multiple indicators may be useful in determining their origins. In addition different indicators can in principle provide information about multiple types of anisotropy that may be present [19].

Here we propose a new indicator, based on the angular pair separation histogram (PASH) method [20], as a measure of large-scale anisotropy. An important feature of this indicator is that it can be used to generate a sky map of large-scale anisotropies in a given CMB temperature fluctuations map. This level of directional detail may also provide a possible additional window into their causes.

The structure of the paper is as follows. In Section II we introduce our Anisotropy Indicator. Section III contains the results of the application of our indicator to the WMAP data, and finally Section IV contains the sum-

*Electronic address: bernui@das.inpe.br

†Electronic address: brunom@cbpf.br

‡Electronic address: reboucas@cbpf.br

§Electronic address: r.tavakol@qmul.ac.uk

mary of our main results and conclusions.

II. ANISOTROPY INDICATOR

In CMB studies the celestial sphere is discretized into a set of equal sized pixels, each with a temperature fluctuation value. Our aim here is to construct an indicator which could measure the departure of CMB temperature fluctuation patterns from statistical isotropy. The first step in constructing this indicator is to order the pixels according to their temperatures and subdivide them into a number of submaps, each consisting of equal number of pixels with similar temperatures. This ordering and subdivision of the CMB map, is motivated by the fact that any anisotropy in the CMB temperature fluctuations implies the presence of uneven distribution of the pixels with similar temperatures.

The next step in constructing the indicator is to generate the pair angular separation histograms (PASH's), which are obtained by counting the number of pairs of pixels in a given submap with angular separation α lying within small sub-intervals (bins), J_i , of $(0, \pi]$, of length $\delta\alpha = \pi/N_{bins}$, where

$$J_i = \left(\alpha_i - \frac{\delta\alpha}{2}, \alpha_i + \frac{\delta\alpha}{2} \right], \quad i = 1, 2, \dots, N_{bins},$$

with the bin centers at $\alpha_i = (i - \frac{1}{2})\delta\alpha$. The PASH is then defined as the following normalized function

$$\Phi(\alpha_i) = \frac{2}{n(n-1)} \frac{1}{\delta\alpha} \sum_{\alpha \in J_i} \eta(\alpha), \quad (1)$$

where n is the total number of pixels in the submap, $\eta(\alpha)$ is the number of pairs of pixels with separation α , and where the normalization condition $\sum_{i=1}^{N_{bins}} \Phi(\alpha_i) \delta\alpha = 1$ holds. Having calculated the PASHs for the submaps we average them at each bin to obtain the mean PASH (MPASH) $\langle \Phi(\alpha_i) \rangle$.

To construct an anisotropy measure, we compare the MPASH with the histogram expected from a statistically isotropic map.¹ The latter can be obtained by randomly generating multiple sets of points distributed isotropically in the celestial sphere and calculating the normalized expected pair angular separation histogram (EPASH) [21] in the form

$$\langle \Phi_{exp}(\alpha_i) \rangle = \frac{1}{N} \frac{1}{\delta\alpha} \sum_{\alpha \in J_i} \langle \eta_{iso}(\alpha) \rangle, \quad (2)$$

where $\langle \eta_{iso} \rangle$ is the average number of pairs of pixels with separation $\alpha \in J_i$ calculated for statistically isotropic

maps, $N = n(n-1)/2$ is the total number of pairs of pixels, and where the coefficient of the summation is the normalization factor. In practice, this is made from scrambled CMB maps.

We denote the difference between the MPASH, $\langle \Phi_{obs}(\alpha_i) \rangle$, calculated from the observational data, and the EPASH $\langle \Phi_{exp}(\alpha_i) \rangle$, obtained from an statistically isotropic distribution of pixels, as

$$\Upsilon(\alpha_i) \equiv \langle \Phi_{obs}(\alpha_i) \rangle - \langle \Phi_{exp}(\alpha_i) \rangle. \quad (3)$$

Now since large-scale anisotropies are nonlocal, we cover the celestial sphere with a number of evenly distributed spherical caps, each defined as a set of points on this sphere whose angular distance from the center of the cap is smaller or equal to a given fixed angle θ_0 (say). We then define our indicator $\sigma = \sigma(\theta, \phi)$ as the variance of $\Upsilon(\alpha_i)$ (which has zero mean), namely

$$\sigma^2(\theta, \phi) \equiv \frac{1}{N_{bins}} \sum_{i=1}^{N_{bins}} \Upsilon^2(\alpha_i). \quad (4)$$

By construction $\sigma(\theta, \phi)$ gives a measure of deviation from isotropy. To further quantify the details of the anisotropy we expand σ (treated as a discrete scalar function on S^2) in spherical harmonics, in the form

$$\sigma(\theta, \phi) = \sum_{\ell=0}^{\infty} \sum_{m=-\ell}^{\ell} b_{\ell m} Y_{\ell m}(\theta, \phi), \quad (5)$$

and calculate the σ power spectrum

$$D_{\ell} = \frac{1}{2\ell+1} \sum_m |b_{\ell m}|^2. \quad (6)$$

It then follows that if a large-scale asymmetry is present in the original temperature distribution, it should significantly affect the σ -map on the corresponding angular scales (i.e. its lower multipoles).

We shall apply the indicator σ to the WMAP data in the next section.

III. APPLICATION TO WMAP DATA

The WMAP measurements have produced high angular resolution maps of the temperature field of the CMB. In such maps the celestial sphere is partitioned in pixels with equal area according to the N_{side} parameter of the HEALPix [22] computational tool. Here we use firstly the full sky WMAP Lagrange-ILC (LILC) map [23] with HEALPix parameter $N_{side} = 128$, corresponding to 196,608 pixels, where to each pixel was assigned a weighted CMB temperature fluctuation. Throughout this paper we use galactic coordinate with equator defined by $b = 90^\circ$.

We calculated σ for a set of 12,288 spherical caps of radius 30° co-centered with the same number of pixels

¹ In practice, a statistically isotropic map is obtained simply by scrambling a given CMB map.

generated by HEALPix with $N_{side} = 32$. The σ -map can then be defined as a scalar function on the celestial sphere which takes the value of σ of each spherical cap at its center. In all the plots reported here, the number of bins chosen to produce PASHs was taken as $N_{bins} = 400$.

Figure 1 shows the Mollweide projection of the σ -map in galactic coordinates obtained from WMAP LILC temperature anisotropy map. As can be seen, it seems to

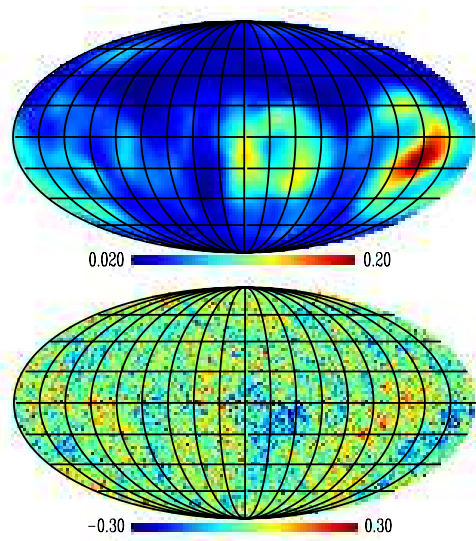


FIG. 1: The full sky map of $\sigma(\theta, \phi)$ calculated from 12,288 evenly distributed 30° caps covering the LILC map. For comparison, the LILC temperature map is also depicted in the bottom panel.

indicate a large-scale anisotropy in the σ -map suggestive of the presence of a dipole-like distribution of anisotropy. Particularly prominent is the very high σ spot concentrated on the south eastern corner of the σ -map with a well defined maximum at $(b \simeq 115^\circ, l \simeq 235^\circ)$. This is in good agreement with the direction recently indicated in Ref. [6, 10] (the separation is about 15°). The comparison of this σ -map with the WMAP LILC temperature map (see the bottom panel in Fig. 1) shows that regions with large temperature contrasts have the highest σ values, as would be expected from the construction of the σ -map.

To obtain more quantitative information about the observed anisotropy, we calculated the power spectrum of the σ -map, which is depicted in Fig. 2. To estimate the statistical significance of these multipole values, we considered a set of 150 Monte Carlo generated statistically isotropic maps and calculated the power spectrum for $\ell \leq 10$ of the corresponding σ -maps. For this range of ℓ , which implies angular separations $\gtrsim 18^\circ$, 768 spherical caps are sufficient to completely cover the celestial sphere. Averaging over the spectra gives the expected power spectrum of the σ -map of a statistically isotropic sky with the same temperature power spectrum as the LILC map. The expected power spectrum thus obtained

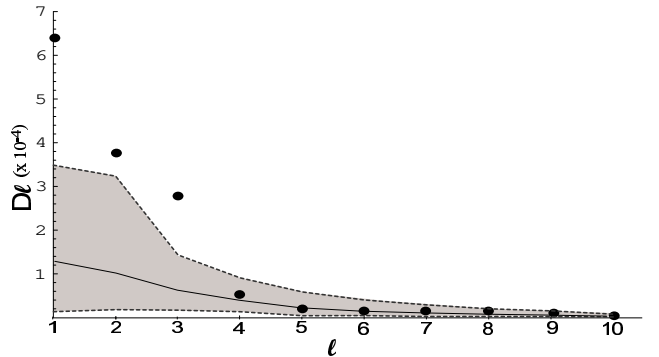


FIG. 2: The power spectrum of the LILC σ -map for $\ell = 1, \dots, 10$ (solid dots). Note the large values of the first three multipoles. For comparison, the means expected σ -map power spectrum for a set of isotropic skies is shown (solid curve), along with its 95% confidence limits (dashed curves).

is also depicted in Fig. 2 (solid line) along with its 95% confidence limits (dashed lines). The actual power spectrum obtained from the LILC σ -map is represented by the solid dots.

We note that the very high dipole value (corresponding to $\ell = 1$) found here, is consistent with the σ -map (see Fig. 1) showing a clear separation of the higher and lower values for σ into roughly two hemispherical regions. Note also the high values of the quadrupole and octopole moments. While the first three multipoles are statistically significantly ($> 95\%$ CL) higher than the expected isotropic power spectrum, the subsequent components all lie very close to the values of the isotropic case.

Given the anisotropic nature of the calculated σ -map, it is worth analyzing the shape of the anomalous multipoles in more detail. To this end, we have depicted in Fig. 3 the dipole, the quadrupole and the octopole, as well as the full σ -map with these three components removed. The analysis of the dipole alone gives a direction towards $(b = 141^\circ, l = 240^\circ)$, which on its own is not in very good agreement with the axis of maximum asymmetry found by [6] and also by [10]. However the sum of the first three multipoles has maximum σ in the direction $(b = 107^\circ, l = 224^\circ)$, which is in much better agreement with the axis of maximum asymmetry suggested in Refs. [6, 10].

The quadrupole component has a very peculiar shape. It appears to be symmetric around an axis slightly off the galactic North-South. With respect to this apparent axis, the minima are at the poles and there is an even maximum region at the equator. To determine this feature more precisely, we used the method proposed in Ref. [5], wherein for each given multipole (in their case, of the temperature map) the direction for which ‘angular momentum dispersion’ is maximized (or, by extension,

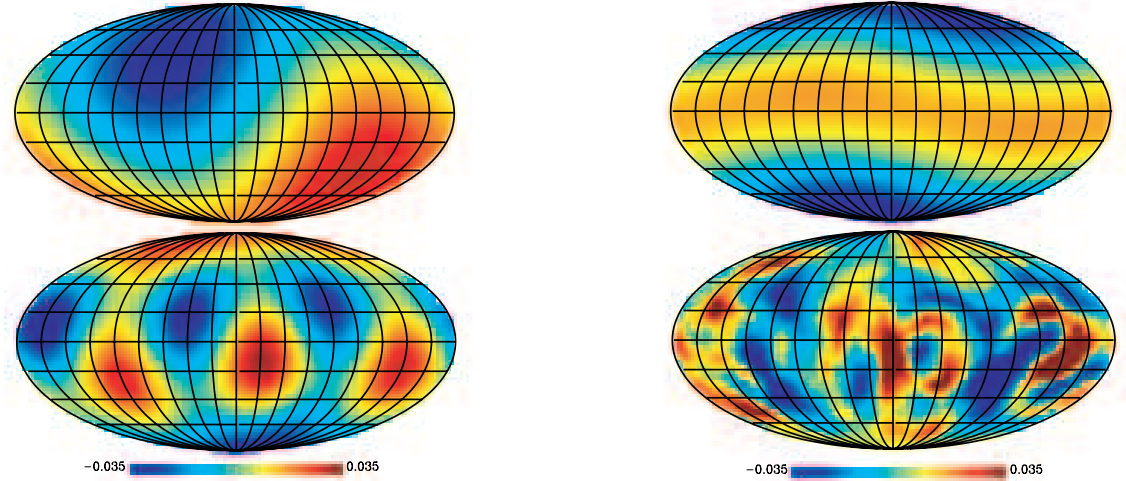


FIG. 3: This figures shows the dipole (upper left), the quadrupole (upper right) and the octopole (lower left) as well as the remaining σ -map with these components removed (lower right).

minimized) is said to be a preferred direction.² Applied to the σ -map, we find that for the quadrupole component the angular momentum dispersion is minimized in the direction ($b = 10^\circ, l = 289^\circ$). We define a new coordinate system (θ', ϕ') considering this direction as the new North-South axis, where we can easily obtain the

coefficients b'_{4m} associated with $Y'_{lm}(\theta', \phi')$. The value of b'_{40} , the only axisymmetric component, is significantly higher than the others, contributing with 82% of the total power in D_l . It is thus clear that this axis is a very good approximation to the axis of symmetry of the quadrupole. Incidentally, it lies somewhat close to the axes of symmetry of the CMB temperature quadrupole and octopole found in Ref. [5] (lying about 24° from both).

The calculation of our anisotropy indicator uses a number of ingredients and parameters whose choice could in principle affect the outcome of our results. To test the robustness of our results, we studied the effects of changing various parameters employed in the calculation of our indicator. We found that the σ -map and its power spectrum do not change appreciably as the number of submaps (in the range 2 to 100) as well as the size of the spherical caps (between 15° and 45°) and their number (greater than 768 corresponding to HEALPix parameter $N_{\text{side}} = 8$) are varied. They are also robust with respect to the number of bins used, in the range 200 to 800, in calculating the histograms.

Given that foreground cleaning algorithms are likely to leave their most pronounced effects in the region of the galactic equator, one may suspect that the pronounced anisotropies found in the σ -map, lying largely close to the galactic equator, are an artifact of the cleaning process. To test this possibility, we calculated the σ -map employing two other CMB temperature maps. The first was the WMAP CO-ADDED map [24], which is the combination of eight (from Q1 through W4) foreground cleaned sky-maps in the frequencies $-Q$, V and W —where galactic contamination is small but still observable (see bottom panel in Fig. 4). The corresponding σ -map is shown on the top panel of Fig. 4, which shows that although new structures emerge around the galactic equator and the spot close to the galactic center is enhanced, the

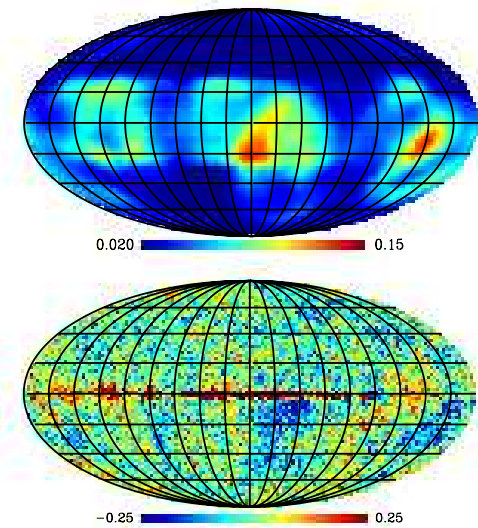


FIG. 4: Full sky map of $\sigma(\theta, \phi)$ for the WMAP CO-ADDED map, showing the effect of unfiltered galactic contamination. Note the hot spot on the southeastern side of the σ -map which remains robust.

² The directions of the maximum and minimum of the angular momentum dispersion are orthogonal. Along with their magnitudes, they fully determine the quadrupole components.

south-eastern 'hot' spot in the σ -map remains almost unchanged in both intensity and location.

We also studied the ‘cleaned’ WMAP (the so-called TOH map) given by Tegmark et al. [4], obtained by using the Wiener foregrounds cleaning algorithm. Again, we found that the main features of the σ -map remain essentially the same. In particular the location of the ‘hot’ spot, as well as other prominent features of the dipole, quadrupole and octopole components of the σ map remain essentially unchanged.

These results seem to indicate that these anisotropic features are independent of the foreground cleaning processes employed.

IV. CONCLUSIONS

We have proposed a new method of directionally measuring deviations from statistical isotropy in the CMB sky, in order to study the possible presence and nature of large-scale anisotropy in the WMAP data.

The use of our anisotropy indicator has enabled us to construct a map of statistical deviations from isotropy for the CMB data. Using this σ -map we have been able to find evidence for a large-scale anisotropy in the WMAP CMB temperature field. In particular we have found, with high statistical significance ($> 95\%$ CL), a small region in the celestial sphere with very high values of σ , which defines a direction very close to the one reported recently [6, 10].

To obtain a more quantitative measure of this anisotropy we studied the spherical harmonic expansion of the σ -map generated from the LILC map and found that the dipole component is significantly higher than would be expected, as compared with an average of a set of Monte Carlo CMB maps generated under the statistical isotropy hypothesis. Moreover, we have found that the combination of the dipole, quadrupole and octopole components of the σ -map has a strongly preferred direction close to the small region of maximum value of σ .

We have shown that the results reported here are robust, by showing that the σ -map does not significantly change by changing various parameters employed in its calculation. We have also studied the effects of

a different foreground cleaning algorithms, or absence thereof, by considering in addition to LILC also the TOH and WMAP CO-ADDED maps. We have found again that the corresponding σ -maps remain qualitatively unchanged. In particular the hot spot on the south-eastern corner of the σ -map remains essentially invariant for all the maps considered here. This robustness demonstrates that our indicator is well suited to the study of anisotropies in the CMB data.

Finally, regarding the origin of such large-scale anisotropy, a number of suggestions have been put forward. A detailed discussion of these suggestions is beyond the scope of the present work. Briefly though, they can arise either from a subtle form of unremoved foreground contamination (in which case the σ -map might indicate where in the sky this contamination is most intense), or from the universe being genuinely anisotropic on large scales. This latter possibility is particularly interesting, as it would have potentially important consequences for the standard inflationary picture, which predicts statistically isotropic CMB temperature fluctuation patterns.

Among the proposed explanations, it has been suggested that the preferred direction could be due to the universe possessing a non-trivial topology [2, 3] (for more details on cosmic topology see the review articles [25], and, e.g., Refs. [26, 27]). If topology is indeed the origin, our indicator would be well suited to distinguish candidate manifolds.

Whatever the origin of these large-scale anomalies may be, the robustness of our anisotropy indicator seems to be sufficiently sensitive to reliably map them, which in turn could facilitate the task of explaining their origin.

Acknowledgements. We thank CNPq, PCI-CBPF/CNPq, PCI-INPE/CNPq and PPARC for the grants under which this work was carried out. MJR thanks Glenn Starkman for fruitful discussions related to statistical isotropy. We are grateful to C.A. Wuensche for his advice on computer simulations. We also thank K. Land and T. Villela for useful comments. We acknowledge use of the Legacy Archive for Microwave Background Data Analysis (LAMBDA). Some of the results in this paper have been derived using the HEALPix package. We also acknowledge the use of the cleaned Tegmark-Oliveira-Costa-Hamilton map.

- [1] C.L. Bennett et al. , *Astrophys. J.* **583**, 1 (2003); C.L. Bennett et al. , *Astrophys. J. Suppl.* **148**, 1 (2003).
- [2] C.J. Copi, D. Huterer, D.J. Schwarz, and G.D. Starkman, [astro-ph/0508047](#).
- [3] D.N. Spergel et al. , *Astrophys. J. Suppl.* **148**, 175 (2003).
- [4] M. Tegmark, A. de Oliveira-Costa, and A.J.S. Hamilton, *Phys. Rev. D* **68**, 123523 (2003).
- [5] A. de Oliveira-Costa, M. Tegmark, M. Zaldarriaga, and A. Hamilton, *Phys. Rev. D* **69**, 063516 (2004); J.R. Weeks, [astro-ph/0412231](#); P. Bielewicz, H.K. Eriksen, A.J. Banday, K.M. Gorski, and P.B. Lilje, [astro-ph/0507186](#).
- [6] H.K. Eriksen, F.K. Hansen, A.J. Banday, K.M. Gorski, and P.B. Lilje, *Astrophys. J.* **605**, 14 (2004).
- [7] E.F. Bunn and D. Scott, *Mon. Not. Roy. Astron. Soc.* **313**, 331 (2000).
- [8] F.K. Hansen, A.J. Banday, and K.M. Gorski, *Mon. Not. Roy. Astron. Soc.* **354**, 641 (2004); F.K. Hansen, P. Cabella, D. Marinucci, and N. Vittorio, *Astrophys. J.* **607**, L67 (2004); T. Wibig and A.W. Wolfendale, *Mon. Not.*

Roy. Astron. Soc. **360**, 236 (2005).

[9] K. Land and J. Magueijo, Phys. Rev. Lett. **95**, 071301 (2005).

[10] K. Land and J. Magueijo, Mon. Not. Roy. Astron. Soc. **357**, 994 (2005).

[11] D.J. Schwarz, G.D. Starkman, D. Huterer, and C.J. Copi, Phys. Rev. Lett. **93**, 221301 (2004).

[12] C.J. Copi, D. Huterer, and G.D. Starkman, Phys. Rev. D **70**, 043515 (2004).

[13] S. Prunet, J.-P. Uzan, F. Bernardeau, and T. Brunier, Phys. Rev. D **71**, 083508 (2005).

[14] E.P. Donoghue and J.F. Donoghue, Phys. Rev. D **71**, 043002 (2005).

[15] E. Komatsu et al. , Astrophys. J. Suppl. **148**, 119 (2003); C.-G. Park, Mon. Not. Roy. Astron. Soc. **349**, 313 (2004); L.-Y. Chiang, P.D. Naselsky, O.V. Verkhodanov, and M.J. Way, Astrophys. J. **590**, L65 (2003); P. Vielva, E. Martinez-Gonzalez, R.B. Barreiro, J.L. Sanz, and L. Cayon, Astrophys. J. **609**, 22 (2004); H.K. Eriksen, A.J. Banday, K.M. Gorski, and P.B. Lilje, Astrophys. J. **622**, 58 (2005); D.L. Larson and B.D. Wandelt, Astrophys. J. **613**, L85 (2004); P. Coles, P. Dineen, J. Earl, and D. Wright, Mon. Not. Roy. Astron. Soc. **350**, 983 (2004); P.D. Naselsky, L.-Y. Chiang, P. Olesen, and O.V. Verkhodanov, Astrophys. J. **615**, 45 (2004).

[16] C. Vale, astro-ph/0510137.

[17] A. Cooray and N. Seto, astro-ph/0509039.

[18] C. Gordon, W. Hu, D. Huterer, and T. Crawford, astro-ph/0509301; K. Tomita, astro-ph/0509518.

[19] T. Souradeep and A. Hajian, astro-ph/0502248; Pramana **62**, 793 (2004), astro-ph/0308002; A. Hajian and T. Souradeep, Astrophys. J. **597**, L5 (2003); A. Hajian, T. Souradeep, and N. Cornish, Astrophys. J. **618**, L63 (2004); A. Hajian and T. Souradeep, astro-ph/0501001.

[20] A. Bernui and T. Villela, astro-ph/0511339.

[21] A.F.F. Teixeira, physics/0312013.

[22] K.M. Górska, E. Hivon, A.J. Banday, B.D. Wandelt, F.K. Hansen, M. Reinecke, and M. Bartelman, Astrophys. J. **622**, 759 (2005).

[23] H.K. Eriksen, A.J. Banday, K.M. Gorski, and P.B. Lilje, Astrophys. J. **612**, 633 (2004).

[24] G. Hinshaw et al., Astrophys. J. Suppl. **148**, 135 (2003).

[25] M. Lachièze-Rey and J.-P. Luminet, Phys. Rep. **254**, 135 (1995); G.D. Starkman, Class. Quantum Grav. **15**, 2529 (1998); J. Levin, Phys. Rep. **365**, 251 (2002); M.J. Rebouças and G.I. Gomero, Braz. J. Phys. **34**, 1358 (2004), astro-ph/0402324.

[26] R. Lehoucq, M. Lachièze-Rey, and J.-P. Luminet, Astron. Astrophys. **313**, 339 (1996); B.F. Roukema and A. Edge, Mon. Not. R. Astron. Soc. **292**, 105 (1997); N.J. Cornish, D. Spergel, and G. Starkman, Class. Quantum Grav. **15**, 2657 (1998); J.R. Bond, D. Pogosyan, and T. Souradeep, Phys. Rev. D **62**, 043005 (2000); J.R. Bond, D. Pogosyan, and T. Souradeep, Phys. Rev. D **62**, 043006 (2000); G.I. Gomero, A.F.F. Teixeira, M.J. Rebouças, and A. Bernui, Int. J. Mod. Phys. D **11**, 869 (2002); H.V. Fagundes and E. Gausmann, Phys. Lett. A **261**, 235 (1999); J.-P. Uzan, R. Lehoucq, and J.-P. Luminet, Astron. Astrophys. **351**, 766 (1999); G.I. Gomero, M.J. Rebouças, and A.F.F. Teixeira, Phys. Lett. A **275**, 355 (2000); G.I. Gomero, M.J. Rebouças, and A.F.F. Teixeira, Class. Quantum Grav. **18**, 1885 (2001); B. Mota, G.I. Gomero, M.J. Rebouças, and R. Tavakol, Class. Quantum Grav. **21**, 3361 (2004); J.-P. Luminet, J. Weeks, A. Riazuelo, R. Lehoucq, and J.-P. Uzan, Nature **425**, 593 (2003); R. Aurich, S. Lustig, and F. Steiner, Class. Quantum Grav. **22**, 2061 (2005); R. Aurich, S. Lustig, and F. Steiner, Class. Quantum Grav. **22**, 3443 (2005); W.S. Hipolito-Ricaldi and G.I. Gomero, astro-ph/0507238.

[27] G.I. Gomero, M.J. Rebouças and R. Tavakol, Class. Quantum Grav. **18**, 4461 (2001); G.I. Gomero, M.J. Rebouças, and R. Tavakol, Class. Quantum Grav. **18**, L145 (2001); J.R. Weeks, R. Lehoucq, and J.-P. Uzan, Class. Quantum Grav. **20**, 1529 (2003); J.R. Weeks, Mod. Phys. Lett. A **18**, 2099 (2003); B. Mota, M.J. Rebouças, and R. Tavakol, Class. Quantum Grav. **20**, 4837 (2003).